Band Edge Structure of PbS, PbSe, and PbTe

JOHN O. DIMMOCK AND GEORGE B. WRIGHT
Lincoln Laboratory, Massachusetts Institute of Technology, Lexington, Massachusetts*

(Received 9 March 1964)

The available experimental data on PbS, PbSe, and PbTe indicate that the valence- and conduction-band extrema of these semi-conductors occur at the L point of the Brillouin zone. The nearly-free-electron model predicts that the valence and conduction states in the vicinity of the forbidden gap at L each consist of three simple spin-degenerate bands. These bands interact strongly with one another and are relatively well isolated from other bands at L. The forms of the dispersion relations, $E(\mathbf{k})$, for these bands are determined using their symmetry and $\mathbf{k}\cdot\mathbf{P}$ perturbation theory, and depend strongly on their order and spacing. The conduction- and valence-band extrema may be either anisotropic, with small, highly concentration-dependent transverse masses, as found in PbTe, or more nearly isotropic, as found in PbS. PbSe is thought to be an intermediate case. The theoretical variation with carrier concentration of the cyclotron masses and extremal cross-sectional areas of the Fermi surface is derived from $\mathbf{k}\cdot\mathbf{P}$ perturbation theory for a simple model of the band structure in PbTe. This model is found to be in good agreement with most of the transport data on PbTe. However, the g factor for the valence band of PbTe, deduced from measurements of the Shubnikov–de Haas effect, is in definite disagreement with the predictions of the simple model, and a consideration of all six bands is necessary in order to obtain complete agreement with experiment. It appears that the band edge structure of PbSe and PbS are similar to that of PbTe with only a difference in the spacing of the various valence and conduction bands.

THE band-edge structure of the lead salts PbS, PbSe, and PbTe has been the subject of considerable experimental work.[1] However, until recently, there has not been sufficient detailed information available on the various band parameters involved to yield a clear picture of the band-edge structure of these materials. There now exist data on de Haas–van Alphen oscillatory magnetic susceptibility,[2] Shubnikov–de Haas oscillatory magnetoresistance,[3–5] Azbel-Kaner cyclotron resonance,[6,7] interband magneto-optical absorption,[8] and on other optical and transport phenomena in these compounds.[9–12] It is the purpose of the present work to consider various models of the band-edge structure of the lead salts and to compare the predictions of the different models with the available data. In as much as possible, we shall follow the logical arguments which have led us to the models discussed below, including the assumptions which have been made. The approach which we have used combines a nearly free electron picture, which determines the symmetry and some general properties of the band functions of interest, with $\mathbf{k}\cdot\mathbf{P}$ perturbation theory,[13] which determines the band parameters to be compared with experiment. This approach results in a parameterized model of the valence and conduction band extrema. The parameters involve the relative spacings of the bands considered, and the momentum matrix elements between these bands. The relative spacings and order of the bands are adjusted to obtain reasonable agreement with the experimental data, and the models considered are those which provide this agreement.

In Sec. I, the symmetry and number of interacting bands in the vicinity of the forbidden gap is determined from the nearly-free-electron picture. Using this information, one can obtain the $\mathbf{k}\cdot\mathbf{P}$ interactions allowed by symmetry.[14] The possible order of the bands in question is discussed and the number of possible arrangements is considered. In Sec. II, the predictions of the various arrangements are considered in the light of the experimental results. A direct allowed-gap four-band model is presented and approximated to a two-band model. The transport properties of the latter model are obtained and found to agree with the experimental results in PbTe and PbSe. The g-factor predictions of this model, however, are found to be in disagreement with experi-

* Operated with support from the U. S. Air Force.

[1] We do not attempt a complete reference list but cite only that work which has been used directly in the present investigation. Many references are contained in the review article by W. W. Scanlon, Solid State Phys. **9**, 83 (1959), and in the proceedings of previous International Semiconductor Conferences.

[2] P. J. Stiles, E. Burstein and D. N. Langenberg, Phys. Rev. Letters **6**, 667 (1961); J. Appl. Phys. Suppl. **32**, 2174 (1961).

[3] K. F. Cuff, M. R. Ellett and C. D. Kuglin, J. Appl. Phys. Suppl. **32**, 2179 (1961); *Proceedings of the International Conference on the Physics of Semiconductors, Exeter* (The Institute of Physics and the Physical Society, London, 1962), p. 316.

[4] M. R. Ellett and K. F. Cuff, Bull. Am. Phys. Soc. **8**, 601 (1963).

[5] R. S. Allgaier, B. B. Houston, and J. R. Burke, Bull. Am. Phys. Soc. **8**, 517 (1963).

[6] P. J. Stiles, E. Burstein, and D. N. Langenberg, in *Proceedings of the International Conference on the Physics of Semiconductors, Exeter* (The Institute of Physics and the Physical Society, London, 1962), p. 577.

[7] R. Nii, J. Phys. Soc. Japan **18**, 456 (1963); **19**, 58 (1964).

[8] D. L. Mitchell, E. D. Palik, J. D. Jensen, R. B. Schoolar, and J. N. Zemel, Phys. Letters **4**, 262 (1963), and to be published.

[9] R. S. Allgaier, J. Appl. Phys. Suppl. **32**, 2185 (1961).

[10] H. R. Riedl, Phys. Rev. **127**, 162 (1962).

[11] J. R. Dixon and H. R. Riedl, in *Proceedings of the International Conference on the Physics and Semiconductors, Exeter* (The Institute of Physics and the Physical Society, London, 1962), p. 179.

[12] R. B. Schoolar, Bull. Am. Phys. Soc. **8**, 516 (1963).

[13] E. O. Kane, Phys. Chem. Solids **1**, 82 (1956).

[14] A partial treatment of this problem has been given by G. L. Bir and G. E. Pikus, Fiz. Tverd. Tela **4**, 2090, 2252 (1962) [English transl.: Soviet Phys.—Solid State **4**, 1530, 1640 (1963)]. These authors neglected the effects of nonparabolicity, which are important, and reached conclusions in disagreement with ours.

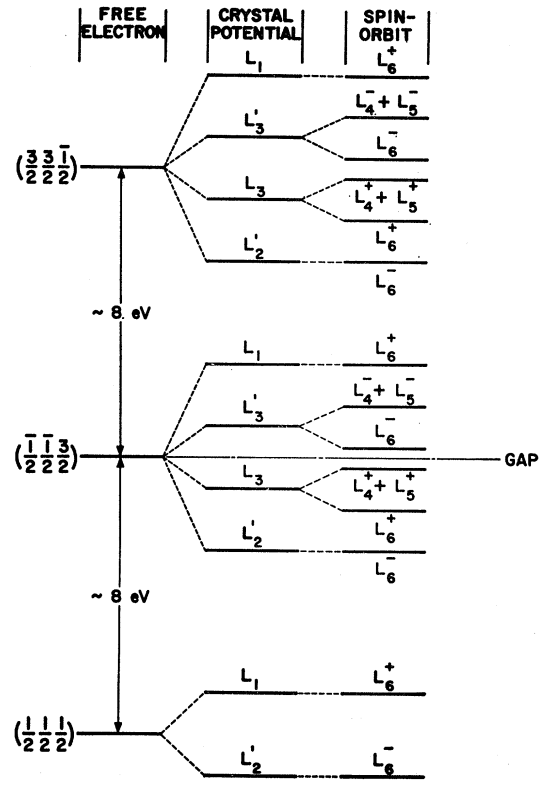

FIG. 1. The low lying states at L in the nearly-free-electron model for a face-centered cubic lattice. The approximate free-electron energies for the lead salts are shown along with a schematic representation of the crystal field and spin-orbit splittings.

ment. It is shown that a more complicated multiband model is necessary to account for the observed transport properties and g factors. In Sec. III, data on PbS, PbSe, and PbTe are compared with the band structure models considered.

I. GENERAL PROPERTIES OF THE VALENCE AND CONDUCTION BANDS IN PbS, PbSe, AND PbTe

All of the experimental data which we have considered seem to be consistent with a model in which the principle conduction- and valence-band extrema in all three compounds PbS, PbSe, and PbTe, are located at the L point (111 edge) of the Brillouin zone.

For a face-centered cubic lattice, the low lying states at L in the nearly-free-electron model with and without spin-orbit interactions are shown schematically in Fig. 1.[15] The lowest set of states arise from the two plane waves of wave vector $\mathbf{k}=\pm 2\pi/a(1/2\ 1/2\ 1/2)$, the central set from the six plane waves of wave vector $\mathbf{k}=\pm 2\pi/a(\bar{1}/2\ \bar{1}/2\ 3/2)$ and cyclic permutations, and the highest set from the six plane waves of wave vector $\mathbf{k}=\pm 2\pi/a(\bar{3}/2\ \bar{3}/2\ 1/2)$ and cyclic permutations. In the free-electron approximation, the energy separation of these states is $\Delta E=2\hbar^2/2m(2\pi/a)^2\simeq 8$ eV for PbS, PbSe, and PbTe, where a is the lattice spacing. The symmetries of the states into which these plane-wave states split under the perturbation of the pseudopotential or crystal field is determined group theoretically and is shown in Fig. 1. Since Fig. 1 is schematic, the order shown is not intended to imply that this is necessarily the order of the bands in the actual crystals, except that we expect the central set of bands to lie near the forbidden gap. In Fig. 1, the L_6 states are doubly degenerate with spin, and the L_4 and L_5 states are degenerate with each other by time reversal. Consequently, all the bands at L are doubly degenerate. Since the crystal structure of PbS, PbSe, and PbTe possesses inversion symmetry, this spin degeneracy is maintained throughout the Brillouin zone. Therefore, we need only consider simple spin-degenerate bands at L. The result is that we expect six simple spin-degenerate bands of symmetries shown in Fig. 1 to lie in the vicinity of the forbidden gap. Of these, three belong to the conduction band and three belong to the valence band.

TABLE I. Symmetry properties of the plane-wave band functions in the vicinity of the atomic sites.

	Cation (Pb)	Anion (S, Se, Te)
$L_6^+(L_1)$	s type	p type
$L_6^-(L_2')$	p type	s type
$L_6^+(L_3)$	d type	p type
$L_{4,5}^+(L_3)$		
$L_6^-(L_3')$	p type	d type
$L_{4,5}^-(L_3')$		

Let us now consider the possible order of these six bands at L. There are $6!=720$ possible different arrangements. Fortunately, many of these can be eliminated by our assumption that the lead salts are direct band-gap semiconductors with their valence and conduction extrema at the L point, since many arrangements result in overlapping valence and conduction bands or in band extrema not at the L point. Also, it seems reasonable to eliminate all arrangements in which the band gap lies intermediate between two states split by spin-orbit interactions. This means that, since the valence and conduction bands must consist of exactly three bands each, the two pairs of spin-orbit split states lie on opposite sides of the forbidden gap (this reduces the number of possible arrangements from 720 to 144). Next, there is evidence that the optical transition across the gap is allowed in all three compounds so that the valence and conduction extrema must be states of opposite parity (reduction 144 to 112).

Since this is still too many to consider in detail, further assumptions must be made. In order to do this, we need more detailed information concerning the six bands in question. In the vicinity of the atomic sites, the band states can be considered to be composed of the

[15] For a discussion of the energy bands for free electrons without spin-orbit coupling in a face-centered cubic lattice, see for example, H. Jones, *The Theory of Brillouin Zones and Electronic States in Crystals* (North Holland Publishing Company, Amsterdam, 1960).

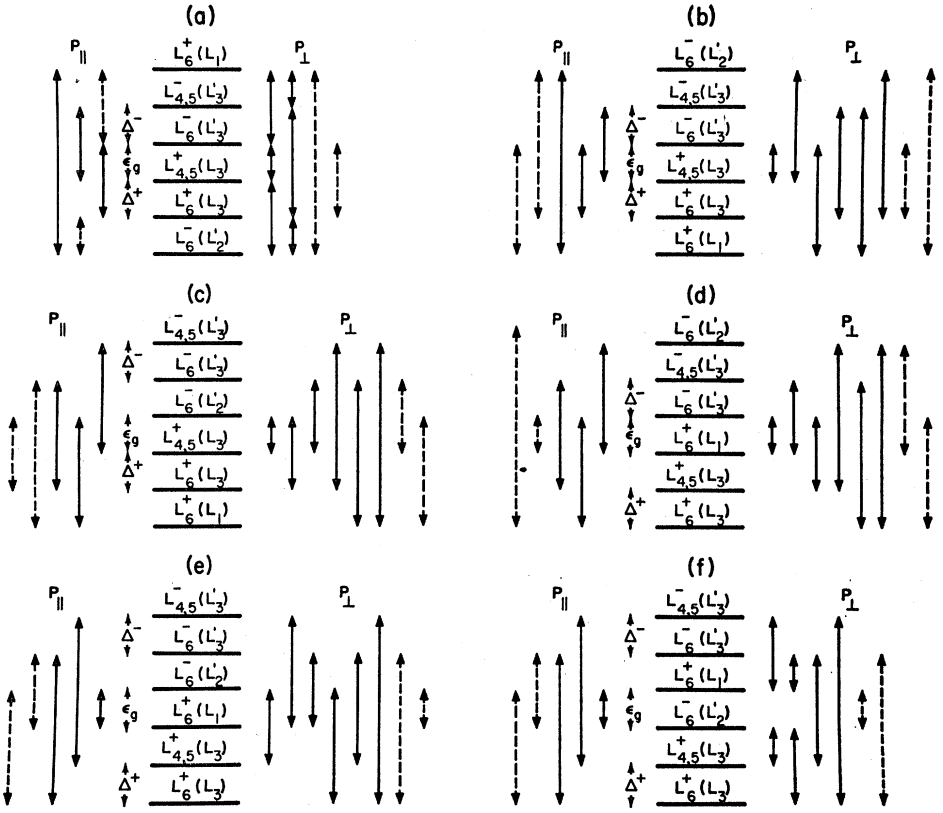

FIG. 2. Possible arrangements of the energy-band states at L in the vicinity of the forbidden gap.

valence states of the free atoms. The general properties can be obtained from the symmetry of the band states in the vicinity of the atomic sites. Taking the origin to be at the Pb site, the results for the states of Fig. 1 are given in Table I. The two lowest lying states of Fig. 1 will be composed, in a tight binding model, of anion and cation s functions. The $L_6^+(L_1)$ state should be mostly cation s type, and the $L_6^-(L_2')$ state should be mostly anion s type. The valence- and conduction-band states should then be mostly p type. The spin-orbit split L_3 state should be made up mostly from anion p functions while the spin-orbit split L_3' state should be made up mostly from cation p functions. Furthermore, the L_6 functions transform like $m_j=\pm\frac{1}{2}$ while the L_4 and L_5 functions transform like $m_j=\pm\frac{3}{2}$.[16] Since the normal order, where the $m_j=\pm\frac{3}{2}$ state lies above the $m_j=\pm\frac{1}{2}$ state, seems to be realized in all semiconductors, with the possible exception of ZnO,[17] we expect the $L_{4,5}^+(L_3)$ state to lie above the $L_6^+(L_3)$ state and the $L_{4,5}^-(L_3')$ state to lie above the $L_6^-(L_3')$ state. This reduces the number of possible arrangements by a factor of 4, leaving us with 28. Again, in the tight binding model we should expect the anion p states to lie below the cation p states, so that the L_3 spin-orbit split state should belong to the valence band and the L_3' spin-orbit split state to the conduction band. The positions of the $L_6^+(L_1)$ and $L_6^-(L_2')$ states are undetermined largely because of the admixture of cation and anion s functions in these bands. This leaves us with 14 distinct possibilities for the order of the valence and conduction bands at L. These are shown in Fig. 2. The diagrams are meant to indicate only the order of the bands and not necessarily their spacings. In the figure, we have indicated the band interactions through the $\mathbf{k}\cdot\mathbf{P}$ perturbation, discussed below, by vertical arrows for $\mathbf{P}$ both parallel and perpendicular to the [111] direction. The solid arrows indicate those interactions which we calculated from the symmetrized plane wave functions. The dotted arrows indicate those additional interactions allowed by symmetry. The forbidden gap is indicated by ϵ_g and the spin-orbit splittings of the L_3, and L_3' states by Δ^+ and Δ^-, respectively. The symbol $L_6^+(L_1)$ for example, indicates a state whose function, including spin, transforms as L_6^+ but which when spin is neglected transforms as L_1. The symbol $L_{4,5}^+(L_3)$ indicates the degenerate pair of states $L_4^+(L_3)$ and $L_5^+(L_3)$. We have not presented separately those cases where the $L_6^+(L_1)$ and $L_6^-(L_2')$ states lie between pairs of spin-orbit split states. For example, in Fig. 2(a), $L_6^+(L_1)$ may also lie between $L_6^-(L_3')$ and $L_{4,5}^-(L_3')$,

[16] See for example, G. F. Koster, J. O. Dimmock, R. G. Wheeler, and H. Statz, *Properties of the Thirty-Two Point Groups* (MIT Press, Cambridge, Massachusetts, 1963).

[17] D. G. Thomas, Phys. Chem. Solids **15**, 86 (1960); J. J. Hopfield, *ibid.* **15**, 97 (1960).

TABLE II. Estimated one-electron spin-orbit splittings for atomic states in Pb, S, Se and Te.

Pb	S	Se	Te	
2.4 eV	0.06 eV	0.35 eV	0.9 eV	p states
0.06 eV	0.002 eV	0.015 eV	0.03 eV	d states

TABLE III. Estimated spin-orbit splittings of the L_3 and L_3' states in PbS, PbSe, and PbTe.

	PbS	PbSe	PbTe
$\Delta^+(L_3)$	0.06 eV	0.24 eV	0.56 eV
$\Delta^-(L_3')$	0.96 eV	0.97 eV	0.98 eV

and $L_6^-(L_2')$ may also lie between $L_6^+(L_3)$ and $L_{4,5}^+(L_3)$. Therefore, Figs. 2(a) and (b) actually each correspond to four possible arrangements; (c) and (d) each correspond to two possible arrangements; and (e) and (f) each correspond to only one possible arrangement giving 14 arrangements in all. If we relax the restriction that L_3 be a valence-band state and L_3' a conduction-band state, we allow 14 additional arrangements which may be obtained simply by inverting the arrangements given in Fig. 2.

Before proceeding with the experimental consequences of the various arrangements and a comparison with the available data, it would be interesting to obtain rough estimates of the spin-orbit splittings Δ^+ and Δ^- for the three compounds, PbS, PbSe, and PbTe. It was first pointed out by Elliott that estimates of the spin-orbit splitting of the band states may be obtained from the atomic spin-orbit splittings of the constitutent atoms.[18] The single-electron atomic spin-orbit splittings for p and d states in Pb, S, Se, and Te have been estimated from the atomic energy levels of the neutral and singly ionized atoms.[19] The values obtained are given in Table II. If one assumes that in IV–VI compounds the electrons in the valence and conduction bands at L spend 40% of their time on the column IV atom and 60% of their time on the column VI atom one can obtain estimates of Δ^+ and Δ^-. The results are shown in Table III. The values for PbTe are in good agreement with those obtained by Johnson, Conklin, and Pratt.[20] It should be noted however, that the numbers given in Table III are intended to be rough estimates only.

II. MODELS FOR THE ENERGY BANDS IN PbS, PbSe, AND PbTe

In order to obtain the experimental consequences of the various band arrangements of Fig. 2, we need to obtain the dispersion relations, $E(\mathbf{k})$, in the vicinity of the L point from $\mathbf{k}\cdot\mathbf{P}$ perturbation theory. Including spin-orbit contributions, this perturbation takes the form,[21]

$$\mathcal{H}'=\frac{\hbar}{m}\boldsymbol{\kappa}\cdot\boldsymbol{\pi}, \tag{1}$$

where

$$\boldsymbol{\pi}=\mathbf{P}+(\hbar/4mc^2)\boldsymbol{\sigma}\times\nabla V. \tag{2}$$

In Eq. (1) $\boldsymbol{\kappa}$ is the wave vector of the state in question measured from the L point. That is $\boldsymbol{\kappa}=\mathbf{k}-2\pi/a$ (1/2 1/2 1/2) where $\mathbf{k}$ is the reduced wave vector of the state. In addition to the standard spin-orbit contribution to the $\mathbf{k}\cdot\mathbf{P}$ perturbation, included in Eq. (2) there will be other relativistic corrections which can be obtained from the one electron relativistic Hamiltonian in a straightforward manner.[22] It is expected that the contribution of these terms to the perturbation should be small[23] and we neglect them here as comparising an unnecessary complication. The matrix elements of $\mathcal{H}'$ can be obtained in parameterized form from the transformation properties of $\boldsymbol{\pi}$, where $\boldsymbol{\pi}$ transforms like the momentum operator $\mathbf{P}$. For $\boldsymbol{\pi}$ parallel and perpendicular to the [111] direction the group theoretical selection rules are given in Table IV and the parameterized matrix elements of $\mathcal{H}'$ are displayed in Table V.[16] In Table V, we have written $\boldsymbol{\kappa}$ in the natural coordinate system for band states at the L point, [111] edge, with $\kappa_z\|[111]$, $\kappa_x\|[\bar{1}\bar{1}2]$, and $\kappa_y\|[1\bar{1}0]$. Table V does not represent a secular determinant but is simply a convenient way of displaying the relevant $\mathbf{k}\cdot\mathbf{P}$ matrix components. It is interesting to consider what simplifications can be made in Table V by assuming various approximations. In general, the spin-orbit interaction mixes the states $L_6^+(L_1)$ and $L_6^+(L_3)$ and the states $L_6^-(L_2')$ and $L_6^-(L_3')$. If we assume that this mixing is small, and that we can also neglect the spin-orbit and other relativistic corrections to Eq. (1), we obtain the result that, in Table V, $\mu=\nu=\xi=\rho=0$. Next, to obtain an estimate of the values of the remaining matrix elements, let us assume that the matrix elements of the $\mathbf{k}\cdot\mathbf{P}$ perturbation are derived principally from the plane-wave portion of the band functions, and that the valence- and conduction-band states in question are given approximately by the appropriate symmetry combinations of the six ($\bar{1}$/2 $\bar{1}$/2 3/2) plane waves. These symmetry combinations are given in Table VI. In the table, the symbol (lmn) represents the function $\exp[2\pi/a(lx+my+nz)]$, where x, y, and z are taken along the principal axes of the crystal. α and β represent spin functions quantized along [111]. The upper signs correspond to the + states and the lower signs to the −

[18] R. J. Elliott, Phys. Rev. **96**, 266 (1954). See also, R. Braunstein and E. O. Kane, Phys. Chem. Solids **23**, 1423 (1962).

[19] C. E. Moore, *Atomic Energy Levels*, Natl. Bur. Std. (U. S.), Circ. No. 467 (1949, 1952, and 1958).

[20] L. E. Johnson, J. B. Conklin and G. W. Pratt, Phys. Rev. Letters **11**, 538 (1963).

[21] G. Dresselhaus, Phys. Rev. **100**, 580 (1955).

[22] See for example, J. Callaway, *Energy Band Theory* (Academic Press Inc., New York, 1964), pp. 46–48.

[23] E. O. Kane, Phys. Chem. Solids **1**, 249 (1956).

TABLE IV. Selection rules for momentum matrix elements at L.

L_i	L_1	L_2	L_3	L_1'	L_2'	L_3'	L_4^+	L_5^+	L_6^+	L_4^-	L_5^-	L_6^-
$\pi_\parallel \times L_i$	L_2'	L_1'	L_3'	L_2	L_1	L_3	L_5^-	L_4^-	L_6^-	L_5^+	L_4^+	L_6^+
$\pi_\perp \times L_i$	L_3'	L_3'	$L_1'+L_2'+L_3'$	L_3	L_3	$L_1+L_2+L_3$	L_6^-	L_6^-	$L_4^-+L_5^-+L_6^-$	L_6^+	L_6^+	$L_4^++L_5^++L_6^+$

TABLE V. $\mathbf{k}\cdot\mathbf{P}$ matrix elements for $(3/2\ \bar{1}/2\ \bar{1}/2)$ states.[a]

	$\lvert L_6^-(L_2')\alpha\rangle$	$\lvert L_6^-(L_2')\beta\rangle$	$\lvert L_6^-(L_3')\alpha\rangle$	$\lvert L_6^-(L_3')\beta\rangle$	$\lvert L_4^-(L_3')\rangle$	$\lvert L_5^-(L_3')\rangle$
$\langle L_6^+(L_1)\alpha\rvert$	$\alpha\kappa_z$	$\mu(\kappa_x+i\kappa_y)$	$\delta(\kappa_x+i\kappa_y)$	$\nu\kappa_z$	$\frac{1}{\sqrt{2}}\zeta(\kappa_x-i\kappa_y)$	$\frac{1}{\sqrt{2}}\zeta(\kappa_x-i\kappa_y)$
$\langle L_6^+(L_1)\beta\rvert$	$\mu(\kappa_x-i\kappa_y)$	$\alpha\kappa_z$	$\nu\kappa_z$	$\delta(\kappa_x-i\kappa_y)$	$\frac{1}{\sqrt{2}}\zeta(\kappa_x+i\kappa_y)$	$-\frac{1}{\sqrt{2}}\zeta(\kappa_x+i\kappa_y)$
$\langle L_6^+(L_3)\alpha\rvert$	$\epsilon(\kappa_x-i\kappa_y)$	$\xi\kappa_z$	$\beta\kappa_z$	$\rho(\kappa_x-i\kappa_y)$	$\frac{1}{\sqrt{2}}\eta(\kappa_x+i\kappa_y)$	$\frac{1}{\sqrt{2}}\eta(\kappa_x+i\kappa_y)$
$\langle L_6^+(L_3)\beta\rvert$	$\xi\kappa_z$	$\epsilon(\kappa_x+i\kappa_y)$	$\rho(\kappa_x+i\kappa_y)$	$\beta\kappa_z$	$-\frac{1}{\sqrt{2}}\eta(\kappa_x-i\kappa_y)$	$\frac{1}{\sqrt{2}}\eta(\kappa_x-i\kappa_y)$
$\langle L_4^+(L_3)\rvert$	$\frac{1}{\sqrt{2}}\theta(\kappa_x+i\kappa_y)$	$-\frac{1}{\sqrt{2}}\theta(\kappa_x-i\kappa_y)$	$\frac{1}{\sqrt{2}}\lambda(\kappa_x-i\kappa_y)$	$\frac{1}{\sqrt{2}}\lambda(\kappa_x+i\kappa_x)$	0	$\gamma\kappa_z$
$\langle L_5^+(L_3)\rvert$	$\frac{1}{\sqrt{2}}\theta(\kappa_x+i\kappa_y)$	$\frac{1}{\sqrt{2}}\theta(\kappa_x-i\kappa_y)$	$\frac{1}{\sqrt{2}}\lambda(\kappa_x-i\kappa_y)$	$-\frac{1}{\sqrt{2}}\lambda(\kappa_x+i\kappa_y)$	$\gamma\kappa_z$	0

[a] $\kappa_z \| [111]$ $\kappa_x \| [\bar{1}\bar{1}2]$ $\kappa_y \| [1\bar{1}0]$.

TABLE VI. Symmetry combinations of plane waves for the valence and conduction bands at L.

State	Function[a]
$L_6^+(L_1)$; $L_6^-(L_2')$	$(1/\sqrt{6})\{(\bar{1}/2\ \bar{1}/2\ 3/2)+(3/2\ \bar{1}/2\ \bar{1}/2)+(\bar{1}/2\ 3/2\ \bar{1}/2)\pm(1/2\ 1/2\ \bar{3}/2)\pm(\bar{3}/2\ 1/2\ 1/2)\pm(1/2\ \bar{3}/2\ 1/2)\}(\alpha$ or $\beta)$
$L_6^+(L_3)$; $L_6^-(L_3')$	$(1/\sqrt{6})\{(\bar{1}/2\ \bar{1}/2\ 3/2)+\omega(3/2\ \bar{1}/2\ \bar{1}/2)+\omega^*(\bar{1}/2\ 3/2\ \bar{1}/2)\pm(1/2\ 1/2\ \bar{3}/2)\pm\omega(\bar{3}/2\ 1/2\ 1/2)\pm\omega^*(1/2\ \bar{3}/2\ 1/2)\}\alpha$
	$(1/\sqrt{6})\{(\bar{1}/2\ \bar{1}/2\ 3/2)+\omega^*(3/2\ \bar{1}/2\ \bar{1}/2)+\omega(\bar{1}/2\ 3/2\ \bar{1}/2)\pm(1/2\ 1/2\ \bar{3}/2)\pm\omega^*(\bar{3}/2\ 1/2\ 1/2)\pm\omega(1/2\ \bar{3}/2\ 1/2)\}\beta$
$L_4^+(L_3)$; $L_5^-(L_3')$	$(1/\sqrt{12})\{(\bar{1}/2\ \bar{1}/2\ 3/2)(\alpha+\beta)+(3/2\ \bar{1}/2\ \bar{1}/2)(\omega^*\alpha+\omega\beta)+(\bar{1}/2\ 3/2\ \bar{1}/2)(\omega\alpha+\omega^*\beta)\pm(1/2\ 1/2\ \bar{3}/2)(\alpha+\beta)$ $\pm(\bar{3}/2\ 1/2\ 1/2)(\omega^*\alpha+\omega\beta)\pm(1/2\ \bar{3}/2\ 1/2)(\omega\alpha+\omega^*\beta)\}$
$L_5^+(L_3)$; $L_4^-(L_3')$	$(1/\sqrt{12})\{(\bar{1}/2\ \bar{1}/2\ 3/2)(\alpha-\beta)+(3/2\ \bar{1}/2\ \bar{1}/2)(\omega^*\alpha-\omega\beta)+(\bar{1}/2\ 3/2\ \bar{1}/2)(\omega\alpha-\omega^*\beta)\pm(1/2\ 1/2\ \bar{3}/2)(\alpha-\beta)$ $\pm(\bar{3}/2\ 1/2\ 1/2)(\omega^*\alpha-\omega\beta)\pm(1/2\ \bar{3}/2\ 1/2)(\omega\alpha-\omega^*\beta)\}$

[a] $\omega=\exp(2\pi i/3)$.

states. Using the functions of Table VI, we obtain the following estimates of the remaining $\mathbf{k}\cdot\mathbf{P}$ matrix element parameters in Table VI:

$$\alpha=\beta=\gamma=(\hbar/m)P_\parallel, \qquad \delta=\epsilon=\zeta=\eta=\theta=\lambda=(\hbar/m)P_\perp, \tag{3}$$

where

$$P_\parallel=(\tfrac{1}{12})^{1/2}(2\pi\hbar/a) \qquad P_\perp=(\tfrac{2}{3})^{1/2}(2\pi\hbar/a). \tag{4}$$

In Fig. 2, the $\mathbf{k}\cdot\mathbf{P}$ interactions calculated from the plane-wave functions are indicated by solid arrows. The additional matrix elements allowed generally by symmetry are indicated by dashed arrows. It will not be necessary at this time to assume the approximate results given by Eqs. (3) and (4). It is of interest, however, to compare the values of $P_\parallel$ and $P_\perp$, which one can obtain by comparing the predictions of the models with the various experimental results, with those values given in Eq. (4).

Let us now develop a model for the valence- and conduction-band structure of PbTe. In p-type PbTe it

appears from various measurements that the cyclotron mass for orbits in a plane perpendicular to the [111] direction is light, $0.02\ m \leq m_\perp \leq 0.05\ m$,[3] where m is the free-electron mass, and strongly dependent on carrier concentration. The longitudinal mass, however, is somewhat heavier, $m_{\parallel} \sim 0.2\ m$, and relatively independent of carrier concentration.[3] This immediately leads to a model in which the transverse effective mass is determined by a band close in energy to the valence band and the longitudinal effective mass is determined by a band somewhat more removed. Approximately the same thing appears to be true for the conduction band in n-type PbTe. The simplest model which includes these effects is a four band model shown in Fig. 3. This model leads to the following $\mathbf{k}\cdot\mathbf{P}$ secular determinant:

$$\begin{vmatrix} \frac{\hbar^2\kappa^2}{2m}+\epsilon_v-\epsilon_g-\epsilon & 0 & \frac{\hbar}{m}P_{\parallel}\kappa_z & \frac{\hbar}{m}P_\perp'(\kappa_x+i\kappa_y) \\ 0 & \frac{\hbar^2\kappa^2}{2m}-\epsilon & \frac{\hbar}{m}P_\perp(\kappa_x-i\kappa_y) & \frac{\hbar}{m}P_{\parallel}'\kappa_z \\ \frac{\hbar}{m}P_{\parallel}\kappa_z & \frac{\hbar}{m}P_\perp(\kappa_x+i\kappa_y) & \frac{\hbar^2\kappa^2}{2m}-\epsilon_g-\epsilon & 0 \\ \frac{\hbar}{m}P_\perp'(\kappa_x-i\kappa_y) & \frac{\hbar}{m}P_{\parallel}'\kappa_z & 0 & \frac{\hbar^2\kappa^2}{2m}-\epsilon_c-\epsilon \end{vmatrix} = 0. \tag{5}$$

Let us consider that ϵ_c and ϵ_v are large compared to the energy ϵ and to ϵ_g. In this case, the four by four secular determinant may be approximated by

$$\begin{vmatrix} \frac{\hbar^2\kappa_z^2}{2m_{\parallel}^c}-\epsilon & \frac{\hbar}{m}P_\perp(\kappa_x-i\kappa_y) \\ \frac{\hbar}{m}P_\perp(\kappa_x+i\kappa_y) & -\frac{\hbar^2\kappa_z^2}{2m_{\parallel}^v}-\epsilon_g-\epsilon \end{vmatrix} = 0, \tag{6}$$

or

$$\frac{\hbar^2}{m^2}P_\perp^2(\kappa_x^2+\kappa_y^2)=\left(\epsilon-\frac{\hbar^2\kappa_z^2}{2m_{\parallel}^c}\right)\left(\epsilon+\epsilon_g+\frac{\hbar^2\kappa_z^2}{2m_{\parallel}^v}\right), \tag{7}$$

where

$$m/m_{\parallel}^c=1+(2P'^2_{\parallel}/m\epsilon_c) \tag{8}$$

and

$$m/m_{\parallel}^v=-1+(2P_{\parallel}^2/m\epsilon_v). \tag{9}$$

In Eqs. (6) and (7), we have assumed that the transverse cyclotron mass in PbTe is small compared to the free-electron mass as indeed it is experimentally. The Fermi surface for a band of the form given by Eq. (7) is a nonellipsoidal figure of revolution about the κ_z axis. Equation (7) actually represents a special case of the Cohen nonellipsoidal model.[24,25] The theoretical variation with carrier concentration of the cyclotron effective masses and extremal cross-sectional areas of the Fermi surface for this model can now be obtained. The extremal cross-sectional area perpendicular to κ_z, that is perpendicular to [111], can be obtained by setting $\kappa_z=0$ in Eq. (7). One then obtains

$$A_\perp=\pi(\kappa_x^2+\kappa_y^2)=\pi(m/\hbar P_\perp)^2\epsilon(\epsilon+\epsilon_g). \tag{10}$$

The corresponding cyclotron effective mass is

$$m_\perp=\frac{\hbar^2}{2\pi}\frac{\partial A_\perp}{\partial\epsilon}=m_{\perp 0}\left(1+\frac{2\epsilon}{\epsilon_g}\right), \tag{11}$$

where

$$m/m_{\perp 0}=2P_\perp^2/m\epsilon_g \tag{12}$$

and $m_{\perp 0}$ is the value of the transverse cyclotron mass at the band edge. Combining Eqs. (10), (11), and (12), we can express the reciprocal of the period [$\alpha=(\text{period})^{-1}$] of the de Haas–van Alphen and Shubnikov-de Haas

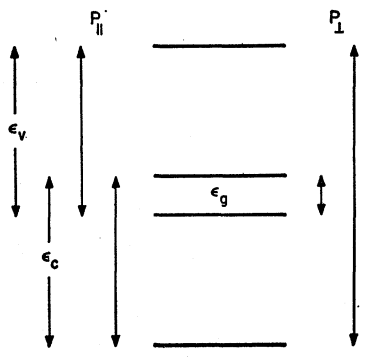

FIG. 3. Four-band model for PbTe.

[24] M. H. Cohen, Phys. Rev. **121**, 387 (1961); see also, D. Weiner, *ibid.* **125**, 1226 (1962).

[25] The Cohen nonellipsoidal model has been applied to the valence band of PbTe by M. R. Ellett, K. F. Cuff, and C. D. Kuglin, Bull. Am. Phys. Soc. **8**, 246 (1963).

oscillations in terms of the cyclotron effective mass:

$$\alpha=(\hbar c/2\pi e)A_\perp=(mc/4e\hbar)\epsilon_g(m_{\perp 0}/m)\times\{(m_\perp/m_{\perp 0})^2-1\}. \quad (13)$$

Equation (13) is valid for both the conduction and valence bands as are Eqs. (10) and (11) if ϵ is measured from the appropriate band edge. The longitudinal extremal cross-sectional area of the Fermi surface of the conduction band is given by

$$A_{\parallel}{}^c=4(2m_{\perp 0}/\hbar^2)^{1/2}(2m_{\parallel}{}^c/\hbar^2)^{1/2}(\epsilon/\epsilon_g)^{1/2}\epsilon\times\frac{(\eta+\gamma)^{1/2}}{3\gamma}\{\eta K(s)+(\gamma-\eta)E(s)\}, \quad (14)$$

where $\eta=(\epsilon+\epsilon_g)/\epsilon$, $s=[\gamma/(\eta+\gamma)]^{1/2}$, $\gamma=m_{\parallel}{}^c/m_{\parallel}{}^v$, and $K(s)$ and $E(s)$ are complete elliptic integrals. For ϵ/ϵ_g small, we obtain

$$A_{\parallel}{}^c=\pi\left(\frac{2m_{\perp 0}}{\hbar^2}\right)^{1/2}\left(\frac{2m_{\parallel}{}^c}{\hbar^2}\right)^{1/2}\left(1+\frac{\epsilon}{\epsilon_g}\right)^{1/2}\times\epsilon\left\{1+\frac{1}{8}\frac{\gamma\epsilon}{\epsilon+\epsilon_g}+\cdots\right\}. \quad (15)$$

The corresponding cyclotron effective mass is

$$m_{\parallel 0}{}^c=(m_{\perp 0}m_{\parallel}{}^c)^{1/2}\left(1+\frac{\epsilon}{\epsilon_g}\right)^{1/2}\times\left\{1+\tfrac{1}{2}\left(1+\frac{\gamma}{2}\right)\frac{\epsilon}{\epsilon+\epsilon_g}+\cdots\right\}. \quad (16)$$

The carrier concentration for the conduction band is given by

$$N=\frac{4}{3\pi^2}\left(\frac{m_{\perp 0}}{m_{\parallel}{}^c}\right)\left(\frac{2m_{\parallel}{}^c\epsilon}{\hbar^2}\right)^{3/2}\left\{1+\left(1+\frac{\gamma}{5}\right)\frac{\epsilon}{\epsilon_g}\right\}. \quad (17)$$

The corresponding expressions for the valence band can be obtained by replacing $m_{\parallel}{}^c$ by $m_{\parallel}{}^v$ and γ by γ^{-1} in Eqs. (14) through (17) if ϵ is measured with respect to the appropriate band edge. Expressions can be obtained from Eq. (7) for the extremal cross-sectional area of the Fermi surface perpendicular to the magnetic field and the corresponding cyclotron mass for arbitrary orientations of the field with respect to the crystal axes. These expressions, however, are reasonably cumbersome. A comparison of the predictions of Eqs. (13) through (17) with experiment is sufficient to determine the band parameters involved.

Finally, let us consider the g factor for the two-band system of Eq. (6). Cohen and Blount[26] have shown that the g factor is directly related to the reciprocal cyclotron mass, for the magnetic field in a given direction, if the appropriate g factor and mass for the band in question are determined by an interaction with one other band only. In the case of the present model, for the magnetic field along κ_z, that is, parallel to the [111] direction, we can use the results of Lax, Mavroides, Zeiger, and Keyes[27] for InSb to obtain

$$\epsilon(\epsilon+\epsilon_g)=(2P_\perp{}^2/m)\{(n+\tfrac{1}{2})\hbar\omega_0\pm\beta_0 H\}, \quad (18)$$

where $\omega_0=eH/mc$, $\beta_0=e\hbar/2mc$ and m is still the free-electron mass. From Eq. (18) and the fact that $\beta_0 H=\frac{1}{2}\hbar\omega_0$, we observe that the spin splitting of a Landau state is equal to the separation between Landau states at the same energy. For large n and small H, the g factor and cyclotron mass can be defined by[27]

$$(e\hbar/m_\perp c)H=\epsilon_{n\uparrow}-\epsilon_{n-1\uparrow} \quad (19)$$

and

$$g_{\parallel}\beta_0 H=\epsilon_{n\uparrow}-\epsilon_{n\downarrow}. \quad (20)$$

Equations (18) and (19) give

$$m_\perp=m(\epsilon_g+2\epsilon)/(2P_\perp{}^2/m) \quad (21)$$

in agreement with Eqs. (11) and (12). For the g factor, Eqs. (18) and (20) give

$$g_{\parallel}=\pm 4(P_\perp{}^2/m)/(\epsilon_g+2\epsilon). \quad (22)$$

Consequently, we find

$$g_{\parallel}m_\perp/m=\pm 2 \quad (23)$$

which is the result obtained by Cohen and Blount.[26]

In Eqs. (10) through (23), we have obtained the predictions of the Cohen two-band nonellipsoidal model [Eqs. (6) and (7)] as applied to the valence and conduction bands of PbTe. Since we expect that actually there will be six bands in the vicinity of the forbidden gap at L, the situation in PbTe is likely to be more complicated than this simple two-band model or the four-band model of Fig. 3. It is therefore of interest to consider the possibility of departures from the two-band model. Since all of the expressions except Eq. (23) contain parameters, which are adjusted in order to obtain agreement between theory and experiment, departures from the two-band model can be absorbed, in part, in these parameters and can consequently be obscured. In fact, the available transport data on PbTe is in agreement with the two-band model, within experimental error, for a particular choice of parameters. In order to obtain a crucial test of the two-band model, we need simultaneous measurements of $m_\perp$ and $g_{\parallel}$ or of the product $g_{\parallel}m_\perp$. This can then be compared to Eq. (23) which contains no adjustable parameters. It is therefore of interest to obtain an expression for $g_{\parallel}m_\perp$ in a more complicated situation than the two-band model. Let us consider, for example, a simple three-band system with

[26] M. H. Cohen and E. I. Blount, Phil. Mag. **5**, 115 (1960).

[27] B. Lax, J. G. Mavroides, H. J. Zeiger, and R. J. Keyes, Phys. Rev. **122**, 31 (1961).

$\kappa_z=0$ for which in the absence of a magnetic field we have

$$\begin{vmatrix} -\epsilon & \frac{\hbar}{m}P_\perp(\kappa_x-i\kappa_y) & \frac{\hbar}{m}P_\perp'(\kappa_x+i\kappa_y) \\ \frac{\hbar}{m}P_\perp(\kappa_x+i\kappa_y) & -\epsilon_g-\epsilon & 0 \\ \frac{\hbar}{m}P_\perp'(\kappa_x-i\kappa_y) & 0 & -\epsilon_c-\epsilon \end{vmatrix}=0. \quad (24)$$

In Eq. (24) we have chosen the phases of the two transverse momentum matrix elements to be different in accordance with the results obtained in Table V from symmetry considerations. Because of this difference, in the presence of a magnetic field parallel to κ_z, Eq. (24) yields

$$\epsilon(\epsilon+\epsilon_g)(\epsilon+\epsilon_c)=(\epsilon+\epsilon_g)(2P_\perp'^2/m)\{(n+\tfrac{1}{2})\hbar\omega_0\mp\beta_0H\} +(\epsilon+\epsilon_c)(2P_\perp^2/m)\{(n+\tfrac{1}{2})\hbar\omega_0\pm\beta_0H\}. \quad (25)$$

In this case the spin splitting of a Landau state is not equal to the separation between Landau states and, instead of Eq. (23), we obtain

$$\frac{g_{11}m_\perp}{m}=\pm2\left\{\frac{(\epsilon+\epsilon_c)P_\perp^2-(\epsilon+\epsilon_g)P_\perp'^2}{(\epsilon+\epsilon_c)P_\perp^2+(\epsilon+\epsilon_g)P_\perp'^2}\right\} \quad (26)$$

in the three-band model. In the limit of small ϵ Eq. (26) reduces to

$$\frac{g_{11}m_\perp}{m}=\pm2\frac{\epsilon_c'-\epsilon_g}{\epsilon_c'+\epsilon_g}, \quad (27)$$

where

$$\epsilon_c'=\epsilon_cP_\perp^2/P_\perp'^2. \quad (28)$$

The inclusion of more bands in the model yields a more complicated expression for $g_{11}m_\perp/m$. The results for small ϵ, however, reduce to equations analogous to Eqs. (27) and (28).

Consider now the transverse g factor for H perpendicular to κ_z. This deviates from $g_\perp=2$ only if the state in question has nonvanishing momentum matrix elements with some other state for both $\mathbf{P}$ parallel to κ_z and for $\mathbf{P}$ perpendicular to κ_z.[27,28] In the four-band model of Fig. 3, no state is connected to any other by both $P_\perp$ and P_{11} so that for this model and for its approximation, the two-band model, the transverse g factors of all states are equal to 2. This is actually a more general property of the system under consideration. From the selection rules for the momentum matrix elements at L given in Table IV we see that the only interaction which is allowed for both $P_\perp$ and P_{11} is $L_6^+\leftrightarrow L_6^-$. Therefore, the transverse g factors for the $L_{4,5}$ states at the L point are equal to 2 from symmetry considerations alone. If we neglect the spin-orbit mixing between the $L_6(L_3)$ and $L_6(L_1)$ states and also the spin-orbit and other relativistic corrections to Eq. (1) we find that all transverse g factors are equal to 2.

Therefore, measurements of $g_\perp$ and of the product $m_\perp g_{11}$ provide the most crucial tests of models of the band edge structure in PbTe. This will also be true for PbS and PbSe. To our knowledge, there has been no measurement of $g_\perp$ for these compounds. The value of $m_\perp g_{11}$ for PbTe has been inferred from measurements of the Shubnikov–de Haas oscillatory magnetoresistance[3,25] and appears to be in disagreement with the prediction, Eq. (23), of the simple four-band model of Fig. 3. This is discussed in more detail in the next section along with a comparison of the remaining data on PbTe with the two-band model. The available data on PbS and PbSe are also compared with tentative models of the band structure in these compounds.

III. COMPARISON WITH EXPERIMENT

The two-band model appears to be in good agreement with the available information on the transport properties of the valence and conduction band extrema in PbTe with the possible exception of the spin splitting of the Landau levels. For this reason, it is felt that a comparison with a more complicated model is not warranted at present.

The two-band model, discussed above, predicts that a plot of the reciprocal of the period of the Shubnikov-de Haas oscillations α against the square of the cyclotron mass $m_\perp$ for a magnetic field along the [111] direction, should yield a straight line [see Eq. (13)]. The comparison of theory and experiment[3] gives the following values for the forbidden gap and transverse valence-band effective mass at the band extrema in PbTe at 4.2°K: $\epsilon_g\simeq0.07$ eV and $m_{\perp0}\simeq0.016m$. Consideration of the multiband model yields a more complicated result. In this case, the plot of α versus $m_\perp^2$ is a straight line only for $\epsilon\ll\epsilon_g$. The data are not sufficiently accurate to indicate any deviation from a straight line. In the multiband model for $\epsilon\ll\epsilon_g$ we obtain Eq. (13) but with ϵ_g replaced by an effective gap. For reasonable spacing of the bands in the multiband model ϵ_g^{eff} differs from ϵ_g by no more than 20% which is less than the error already present in the determination of ϵ_g from a comparison of the two-band model and experiment.

If we estimate the ratio of longitudinal valence- and conduction-band masses to be $\gamma^{-1}=m_{11}{}^v/m_{11}{}^c\simeq1.5$, a comparison of Eq. (15) with experiment[3] yields $m_{11}{}^v\simeq0.18\ m$. Using these values for the band parameters, we can obtain $m_\perp$ as a function of concentration from Eqs. (17) and (11).[29] The result is in good agreement with the data of Cuff, Ellett, and Kuglin, except at their highest concentration. Using Eq. (12) and the

[28] L. M. Roth, Phys. Rev. 118, 1534 (1960).

[29] It is interesting to observe that Eqs. (11) and (17) yield a dependence of $m_\perp$ on N which can be approximated by $m_\perp\approx N^{\frac{1}{3}}$ over a considerable range of N.

values of ϵ_g and $m_{\perp 0}$ obtained above we find that for PbTe at 4.2°K, $2P_\perp^2/m \simeq 4.5$ eV. The value obtained from the nearly-free-electron model, Eq. (4), is $2P_\perp^2/m = 9.95$ eV. Considering the approximations made, the agreement between these two numbers is not unsatisfactory. An estimate of $P_{\parallel}$ can not be obtained since we do not know the values of ϵ_c or ϵ_v in Eqs. (8) and (9).

One can show[26] that the spin splitting of the Landau levels introduces a multiplicative factor of $\cos(r\pi g m_c^*/2m)$ in the amplitude of the de Haas–van Alphen oscillations, and presumably also in the Shubnikov–de Haas oscillations. Therefore, although there are no direct measurements of the g factor in PbTe, one can obtain an estimate of the product $m_c^* g$ by comparing the amplitude of the fundamental oscillations ($r=1$) with that of the second harmonic ($r=2$). The observation that the fundamental vanishes in favor of the second harmonic for H parallel to [111] can be accounted for if

$$g_{\parallel} m_\perp / m \simeq (2n+1) \tag{29}$$

where n is an integer. This situation seems to exist in the valence band of PbTe,[3,30] and disagrees completely with the prediction of the two-band model, Eq. (23). It is therefore necessary to consider more complicated models of the valence and conduction band structure of PbTe. The simple two-band model which we have been examining can be considered as a simple approximation to the band arrangements shown in Figs. 2(a) through (d). A consideration of Eq. (27) shows that a value of $g_{\parallel} m_\perp/m = \pm 1$, ($\epsilon_c' = +3\epsilon_g$) is consistent with the arrangements shown in Figs. 2(b), (c), and (d) and not with Fig. 2(a) whereas a value of $g_{\parallel} m_\perp/m = \pm 3$, ($\epsilon_c' = -5\epsilon_g$) is consistent only with Fig. 2(a). It is obvious, therefore, that a direct measurement of $g_{\parallel}$ in p-type PbTe would greatly aid in the determination of the band structure of this compound.

The available information on the conduction and valence bands in PbSe is not as complete as that for PbTe. Consequently, we can offer only a tentative model for the band structure in this compound. Ellett and Cuff[4] have reported the observation of Shubnikov–de Haas oscillatory magnetoresistance in both n- and p-type PbSe. It appears from their work that the valence- and conduction-band extrema in PbSe are quite similar to those of PbTe. In p-type PbSe, for example, at a concentration of 2×10^{18} cm^{-3} they report a transverse cyclotron mass of 0.047 ± 0.005 m, to be compared with about 0.035 m in PbTe at the same concentration.[3] The anisotropies for these two compounds, however, are rather different being 2.0 ± 0.2 in PbSe and 7 ± 1 in PbTe at this concentration. This indicates that, perhaps, the four-band model of Fig. 3 is applicable to PbSe as well. However, in this case, since the mass anisotropy is not large, it appears that ϵ_c and ϵ_v are not much larger than ϵ_g such that the two band model is not a good approximation in PbSe. Further evidence[4] of this more complicated situation is that whereas $m_\perp$ increases markedly with increasing concentration the anisotropy decreases only slightly indicating that the longitudinal mass also increases with concentration. The Fermi energy in PbSe at concentrations of 10^{18}–10^{19} cm^{-3} must be comparable not only with ϵ_g, as was the case in PbTe, but also with ϵ_c and ϵ_v. We, therefore, tentatively conclude that in PbSe there should exist multiple valence and conduction bands close to the respective band edges. There is some evidence of this also from optical measurements.[12]

The conduction band in PbS appears to be even more isotropic than that of PbSe. The number of carriers calculated from the observed cross-sectional areas of the Fermi surface is only about one-quarter of that determined from Hall measurements.[2,5] This indicates that the conduction band edge in PbS also occurs at the L point ([111] edge). The observed isotropic mass can be accounted for if one considers multiple valence and conduction bands. It seems, therefore, that the valence- and conduction-band structure of PbS is qualitatively the same as that of PbSe and PbTe and that a multiple-band model is necessary to explain the data.

IV. CONCLUSION

All of the existing data on the conduction and valence bands in PbS, PbSe, and PbTe are consistent with a model for the band structure of these compounds in which the principal valence- and conduction-band extrema occur at the L point ([111] edge) of the Brillouin zone. From a nearly-free-electron picture, we found that there should be six bands in the vicinity of the forbidden gap at L and that three of these are conduction bands and three are valence bands. A simple four-band model was proposed for the valence and conduction bands in PbTe. This was further simplified to a two-band model which is a special case of the Cohen nonellipsoidal model for the band structure in bismuth. This two-band model was found to be in good agreement with most of the transport data for PbTe. However, the g factor for the valence band of PbTe deduced from the Shubnikov–de Haas oscillations, is in definite disagreement with the predictions of either the two- or four-band models and it is necessary to consider all six bands in order to obtain complete agreement with experiment. It appears that the band-edge structure in PbSe is quite similar to that of PbTe and that the simple four-band model proposed for PbTe may be applicable to PbSe as well. However, in this case, the energy spacings of all four bands are comparable to the Fermi energy such that in PbSe the four-band model may not be approximated by the Cohen two-band model. We, therefore, tentatively conclude that in PbSe there should be at least four closely spaced bands comprising the conduction and valence band edges. The situation in PbS also appears complicated. Although presently

[30] Y. Shapira and B. Lax, Phys. Letters **7**, 133 (1963).

available evidence is not conclusive, it appears that the band edge structure of PbS may be similar to that of PbSe and PbTe with only a difference in the spacing of the various valence and conduction bands.

In conclusion, we should like to indicate what information would be most useful in further determining the details of the valence and conduction bands in PbS, PbSe, and PbTe. Obviously, more complete and detailed information on the cyclotron masses and extremal cross-sectional areas of the Fermi surface of these compounds as a function of concentration would enable one to obtain a more critical comparison with the proposed band structure models. Also, of course, more complete optical and magneto-optical data would be very useful. One of the principal results of the present investigation is, however, that measurements of the g factor in these compounds would provide rather crucial information on their band structures. We saw, using symmetry arguments and a minimum of assumptions, that $g_\perp$, the g factor for a (111) band for a magnetic field perpendicular to the [111] direction, is equal to 2. The observation of a large deviation from 2 would indicate that the band being observed is an L_6 band and in addition that relativistic effects are important in the $\mathbf{k}\cdot\mathbf{P}$ perturbation. We also saw that the simple two- and four-band models proposed for PbTe and PbSe made definite predictions for g_{11}. A deviation from this prediction seems to occur in PbTe and probably also occurs in PbSe. A direct measurement of g_{11} in these compounds would also provide useful information. More complete data is necessary before a detailed comparison can be made.

Note added in proof. After this paper was submitted, the authors received an unpublished report of a pseudopotential calculation for PbTe by L. Kleinman and P. J. Lin. They obtain essentially the band order shown in our Fig. 2(d) and state that the spin orbit mixing of the L_6^- states is large. This means that the dotted interactions shown in Fig. 2 should be important. This also indicates that our simple model for PbTe, Fig. 3, may be inadequate in that a longitudinal interaction between the valence and conduction bands should be included. We should also mention that interband magneto-absorption studies of epitaxial PbS, PbSe, and PbTe have recently been carried out by Mitchell, Palik, and Zemel. They obtain a gap in PbTe at 4.2°K of 0.19 eV in apparent disagreement with our estimate of $\epsilon_g=0.07$ eV based on a comparison of the two band model with the data of Cuff, Kuglin, and Ellett.[3] Although the value of $\epsilon_g=0.07$ eV gives the best fit to this data, a value as large as $\epsilon_g=0.16$ eV and $m_{\perp 0}=0.022m$ is consistent with the data within the quoted experimental accuracy. The authors would like to thank D. L. Mitchell, E. D. Palik, and J. N. Zemel, and L. Kleinman, and P. J. Lin for sending us their results prior to publication.

ACKNOWLEDGMENTS

The writers wish to express their appreciation to H. J. Zeiger for many helpful conversations, and to D. H. Mitchell, E. D. Palik, and Y. Shapira for interesting discussions of their experimental data. We also wish to thank V. J. Mason and W. C. Mason for supplying the closed form expression for A_{11}^c, Eq. (14).